Proceedings for the 2018 EUMETSAT Meteorological Satellite Conference,
17-21 September 2018, Tallinn, Estonia

ON THE SENSITIVITY OF NOWCASTING ALGORITHMS FOR CONVECTIVE INITIATION IN SATELLITE IMAGES TO AUTOMATIC TRACKING TECHNIQUES

Stephan Lenk[(1)], Fabian Senf[(1)], Hartwig Deneke[(1)] and Katja Hungershoefer[(2)]

(1) Leibniz Institute for Tropospheric Research (TROPOS), Permoserstr. 15, 04318 Leipzig, Germany
(2) German Weather Service (DWD), Frankfurter Straße 135, 63067 Offenbach/Main, Germany.

Abstract

The reliable detection of clouds that will develop into thunderstorms is of high interest in operational weather forecasting. Satellite based detection algorithms for convective initiation are considered a promising avenue to improve the nowcasting of thunderstorms. The thunderstorm detection indicators with the highest information content for convective growth in its early stage within these algorithms are the Lagrangian time trends of cloud properties. Reliable thunderstorm tracking techniques are needed to determine them properly. Hence, the tracking technique used has a large impact on the overall detection capability. Therefore, this study explores four different automatic cloud tracking techniques and their applicability to the task of quantifying the temporal evolution of cloud properties within the detection algorithms and reports preliminary results for a set of cases in Central Europe.

INTRODUCTION

The nowcasting of thunderstorms, i.e. the prediction of thunderstorms for a time horizon of up to one hour, is an important task of operational weather forecasting. Often a combination of different data sources, e.g. weather radar, satellite, radiometer and numerical weather prediction models (NWP), is used for this purpose. With the improving spatial and temporal resolution of satellite instruments the detection capabilities have improved over the last few decades. Geostationary satellites offer the chance to observe growing convective clouds also during the early stages of the convective life cycle. A number of different approaches have been developed over the years to detect convective initiation (CI) with the help of satellite data. The first operational algorithms for satellite based CI detection have been developed for the North American GOES (Geostationary Operational Environmental Satellite) satellite series (Roberts & Rutledge, 2003; Mecikalski & Bedka, 2006; Walker et al., 2012). Efforts have been made to adapt these algorithms to METEOSAT SEVIRI (Spinning Enhanced Visible and InfraRed Imager) instruments (Siewert et al., 2010), which, to our knowledge, are currently only applied within the demonstrational NWC SAF CI product (Autonès & Moisselin, 2016). Within such algorithms an important class of indicators consists of the Langrangian time trends of cloud properties. To determine these indicators correctly a reliable cloud tracking approach is needed. Most publications concerning satellite based CI detection algorithms comment only shortly on this topic. A commonly used approach is the derivation of cross correlation based atmospheric motion vectors (AMV). First developed and applied by Fujita et al. (1969), AMVs have been continuously enhanced and are nowadays widely assimilated into atmospheric models. They are also used as the base of CI detection algorithms. As the cross correlation approach is a pattern matching algorithm, it has some shortcomings, when cloud fields change rapidly, which is often the case for convective clouds. Moreover, the current implementations of the approach are tuned for usability in NWP, which limits the applicability for the use in CI detection algorithms (Bedka & Mecikalski, 2005). Another alternative approach, used for the second generation of CI detection algorithms, is object tracking (Walker et al., 2012; Senf & Denke, 2017; Patou et al., 2018). The basic idea for object tracking of cloud objects has also been applied before successfully (Arnaud et al., 1992; Machado et al., 1998; Mathon & Laurent, 2001), but also has shortcomings in the early phase of the convective life cycle, too. Another interesting class of field-based tracking approaches being able to track clouds even in the very early phase of the convective life cycle, is the class of optical flow

algorithms. They extent the basic principle of the cross correlation tracking and also allow tracking fields with flow discontinuities making them potentially interesting for the tracking of convective clouds. They are not as widely used to track clouds as the cross correlation and the object tracking but there have been recent promising attempts (Wu et al., 2016; Urbich et al., 2018) using the approaches after Farnebäck (2003) and Zach et al. (2007). In this study we therefore aim to compare two optical flow algorithms (Farnebäck, 2003; Zach et al., 2007) with a cross correlation and an object tracking to identify their strengths and weaknesses and to ultimately improve the tracking of convective clouds and thus help to improve the detection capability of satellite-based CI detection algorithms.

The outline is as follows. The data and the method used are desribed first before the results are discussed. A conclusion and outlook section then concludes this paper.

DATA

This study combines infrared rapid scan service (RSS) observations of the SEVIRI instrument on board of EUMETSAT's METEOSAT second generation satellites with ground based observations of the German weather radar network operated by the German Weather Service. From the available SEVIRI channels only the IR-10.8-µm channel with an approximate ground resolution of 3 km $\times$ 6 km over Central Europe and the high resolution visible channel (HRV) with a ground resolution of about 1 km $\times$ 2 km over Central Europe have been considered. As radar data the radar reflectivity data of the precipitation scan which are available as the RADOLAN-RX composite product. This product combines the scans of all German C-band radars and has a ground resolution of 1 km $\times$ 1 km and a temporal resolution of 5 min.

Using satellite data from the year 2013, a manually selected data base of cases with convective development has been created. Focusing on isolated convective cells without splits and merges only, such objects have been identified visually in IR-10.8-µm brightness temperature maps. The object minimum point has than been tracked backward in time starting from the largest anvil extent until the cloud could not been distinguished visually from the background any more. A total of 142 tracks of isolated convective objects have been obtained. The cloud tracks then have been parallax corrected using cloud height information from the NWC SAF Cloud Height Product and have been projected onto the radar data from the RADOLAN RX composite. To determine the time step of convective initiation (CI) a radar based reflectivity threshold was choosen. As pointed out in Haberlie et al. (2015) a list a number of radar based definitions for CI are possible. We have chosen a threshold of 35 dBZ which is often used in other studies (e.g. Roberts & Rutledge, 2003). Using this threshold, the CI time and location for all the tracks was determined and then used as reference point for the subsequent analyses. The geographical location of the 142 CI events is shown in Figure 1.

METHODS

In the following section the tracking approaches used and the evaluation strategy are introduced.

Tracking approaches

Starting from the CI points introduced presented in the Data section, tracks of the isolated convective clouds have been created for a time frame of 30 min both into the future and past using the different approaches. First, the tracks have been determined manually by visually following (identifying them in subsequent images the clouds in the IR-10.8-µm images and assigning track points to the minima in the brightness temperatures of the clouds. In the second step, tracks were determined using four different approaches of automatic tracking:

1. cross correlation tracking
2. optical flow approach after Farnebäck (2003)
3. TV-L1 optical flow approach after Zach et al. (2007)
4. overlap object tracking approach

Each method was applied to the IR-10.8-µm and HRV channel. The result is discussed in the next section.

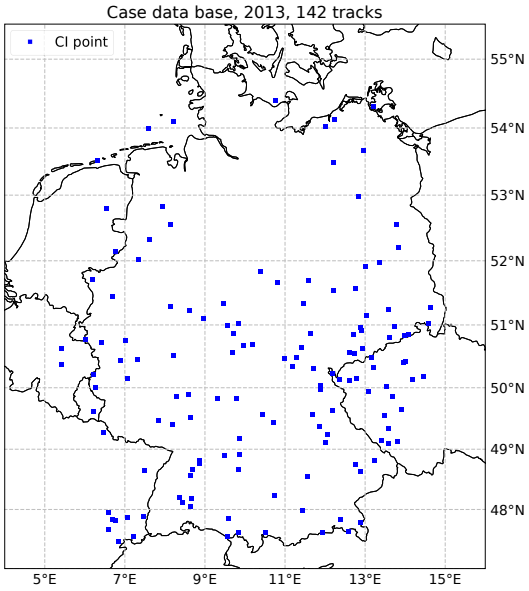

Figure 1: **Map of the case data base used for the analysis. The blue dots denote the CI points, i.e when a radar signal of 35 dBZ was reached in the radar data.**

A schematic illustration of the different approaches is given in Fig. 2. The cross correlation tracking approach forms the basis of atmospheric motion vector (AMV) algorithms used widely to estimate atmospheric motion from weather satellite images. One example is the NWC SAF HRW product (Pereda & Calbet, 2016). In this study the implementation following Guizar-Sicairos et al. (2008) was used which is part of Python's scikit-image package (Van der Walt et al., 2014). The basic idea is to determine a displacement vector which minimises the sum-of-squared differences of the two images, or in other words, maximises their cross-correlation. The scikit-image implementation utilises the phase correlation matrix of the two images for this purpose, whose maximum corresponds to the shift between the two images (Fig. 2 top right). This algorithm allows to determine sub-pixel shifts and can be applied to sub-regions of the image. As convective clouds usually develop and change rapidly, the family of optical flow approaches, which is an extention to the cross correlation tracking might be better suited to track convective clouds and are investigated as an alternative possibility here. The optical flow algorithms deliver a dense field of motion vectors for all image pixels (Fig. 2 centre right). One approach considered in this study, is the optical flow after Farnebäck (2003). Following this approach, the motion is infered by approximating the motion within the neighbourhood of a pixel by a quadratic polynomial. This approach is rather fast in terms of computation time, but is not able to handle flow discontinuities. An alternative approach which is able to mitigate flow discontinuities is presented by Zach et al. (2007). It uses the total variation (TV) regularisation of the L1 norm applied to the distance to derive a motion esimate, which is considered to be more robust to outliers. In this study the Python interface to the opencv implementations of the Farnebäck and TV-L1 algorithms (Janku et al., 2016) have been used.

Both the cross correlation and the optical flow algorithms have a number of parameters which need to be chosen to obtain the best accuracy for any particular applications first. To estimate these parameters the standardised MPI Sintel Dataset (Butler et al., 2012) has been used. Different sets of parameters have been tested against the reference flow and the set with the smallest deviation from the reference has been selected for the further analysis.

Another approach used in this study is object tracking. For this purpose a suitable object definition is needed (Fig. 2 red boundaries), and the relationship of objects in subsequent images has to be determined. In this study, an adaptive hysteresis thresholding has been applied to obtain the objects. Fig. 3 illustrates the principle for an example of IR-10.8-µm brightness temperature data. Hysteresis thresholding involves two thresholds. Taking the histogram of the values of a satellite scene, the first one is used to separate potential objects from the background (Fig. 3, red line). We have found that the cross correlation based thresholding approach after Yen et al. (1995) works well to separate interesting isolated convective cloud objects from the background.

Then a second threshold is applied to eliminate object candidates by only retaining objects with a regions above a second threshold. From our experience taking the first percentile works to capture most of the objects tracked in the manual reference tracks in HRV data and the fifth percentile to capture the objects in IR-10.8-µm data for the time step of the start point (Fig. 3, blue line). Then the possible objects have been related to each other in subsequent images if they overlaped. Using the object sequences obtained this way, the object centroids where connected to one object track. Since this study focuses on isolated convection, tracks with splits and merges have not been considered here.

All approaches analysed in this study are pattern matching algorithms and therefore work best if the structures do not change too much between two images.

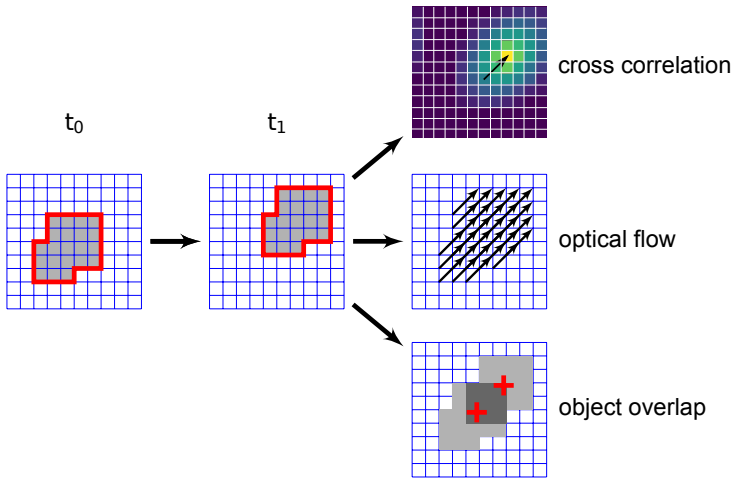

Figure 2: **Schematic illustration of the different tracking approaches. Given a rather simple, not changing object (grey) moving from t_0 to t_1 by two pixels up and right the three different tracking approaches return different results. The cross correlation approach returns one movement vector for the whole object whereas the optical flow approaches can return movement vectors for all object pixels. The object tracking approach also returns only one movement vector for the object but is quite versatile in which point of the object to track (here the object centroid given by the red crosses).**

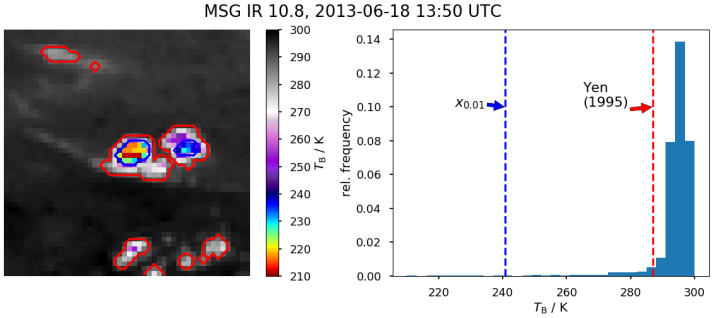

Figure 3: **Principle of the hysteresis thresholding used for the object tracking method. Taking two thresholds (red and blue lines in the left panel and contours in the right panel), the image is segmented into background and objects.**

Evaluation of the tracking approaches

The different tracking approaches illustrated in the previous section have been evaluated in two ways. First, to evaluate the tracking accuracy, it has been determined how far the tracks from the automatic tracking techniques deviate from the ones manually tracked by analysing the end point error of the automatic tracks. The end point error is defined as the Euclidian distance (ϵ_e) of the automatic tracking points and the manual ones (Eq. 1) with the manual track being the reference (ref in Eq. 1).

$$\epsilon_e = \sqrt{(x_{ref} - x)^2 + (y_{ref} - y)^2} \tag{1}$$

Second, it has been evaluated how well the life cycle of the convective clouds is represented by the automatic tracking techniques. To do so, the median life cycle of all manual and automatic tracks where compared.

RESULTS

Tracking accuracy

As shown in Fig. 4, the end point errors of the different tracking techniques follow similar trends for the field-based tracking techniques, but look substantially different for the object tracking. As expected, the end point error increases with time with respect to the reference point. Looking at the median, no clear differences for tracking forward or backward in time can be identified. Instead, the tracking errors are distributed quite symmetrically around the starting point. On the other hand, the position uncertainty is larger at the beginning of the track. This is reasonable, because clouds are often quite small and thus cannot be resolved well by the SEVIRI instrument at the beginning of the convective life cycle. In addition, several smaller clouds often merge into one larger convective cloud or are covered by an anvil and thus are perceived as one cloud. This hampes the derivation of correct movement vectors in the early phase of the convective life cycle, as it is difficult to decide which cloud to track.

The end point error of the object tracking is distinctly higher than for the field-based techniques for both channels. One reason for this is, that the linking of the objects sometimes links different convective cells into one object, when they share an overlap. This happens especially in the early stage, when one object dies but has an overlap with another object in a neighbouring time step. Then the wrong object is tracked further and thus the tracking error increases. A second reason is, that, when the objects are large, the convectively active part of the cloud can be distant from the object centroid. This leads to an increased tracking error, too. Except for the very early stage, the error of the object tracking in the HRV channel is lower than for the IR-10.8-µm channel. This is probably due to the fact, that the higher ground resolution of the HRV channel allows a better discrimination of objects.

The tracking errors obtained for field-based tracking techniques are in the order of three to four SEVIRI standard resolution pixels over Central Europe and thus relatively low. The differences between the analysed tracking techniques are quite small, especially for the IR-10.8-µm channel. All examined field-based tracking techniques thus seem to be equally suited for the tracking of convective clouds at this stage. However, there are some small differences. When tracking on the HRV channel, the cross correlation tracking has the highest error whereas the optical flow techniques and the object tracking have smaller errors, despite the early phase of the considered time range. This difference is probably due to the texture fluctuations in the HRV channel. The optical flow algorithms seem to be able to cope better with this. For the largest part of the considered time frame the TV-L1 flow hast the lowest error but in the early stage its error increases more than for the other field-based techniques. In this stage the Farnebäck optical flow has the lowest error, which is probably due to the stronger smoothing prior to the flow calculation of this algorithm.

Representation of the convective growth phase

When evaluating the resulting representation of the convective growth phase (Fig. 5), the different field-based tracking approaches again lead to comparable results, whereas results from our object tracking are rather different. Looking at the tracking of the IR-10.8-µm channel, all field-based techniques yield a reasonable representation of the convective growth phase: starting from a rather warm cloud, the cooling results in a colder thus higher cloud. A good representation to the life cycle obtained from the visual tracking is found in the center part of the considered time frame. In the early phase, the representation the automatic tracking seems to be even better than the one from visual tracking. Especially in this early stage, it is often hard to visually distinguish the cloud and thus the visual tracking is very error prone. In the later phase of the life cycle, the differences between the field based tracking techniques increase. The TV-L1 optical flow tracking follows visual tracking quite nicely whereas the other techniques deliver warmer median cloud top temperatures. In this later stage of the life cycle the clouds have quite a large extent but the convective parts are rather limited in extent.

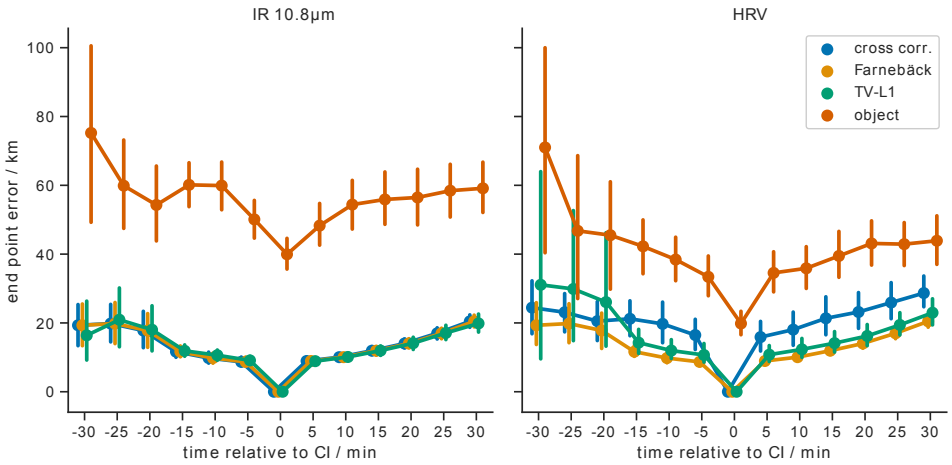

Figure 4: **Median end point error (dot) and inter quantile range (error bar) for all database case for the different tracking techniques obtained for IR-10.8-µm (left) HRV fields (right). The end point error curves have been shifted on the time axis for the different techniques to enhance the visibility but belong to the same time steps.**

Looking at the tracking on the HRV channel, the differences between the automatic tracking techniques are similar but a bit larger. This is due to the larger textural fluctuations in the solar channels and the higher spatial resolution. Location differences of just a few pixels can lead to rather large differences in reflectance. The overall trend shows an increase in cloud reflectance but not as pronounced as the cooling in the IR-10.8-µm channel. However, this is was to be expected, as the cloud reflectance does not only dependend on the cloud height.

The results of median object tracking are not really comparable to the results of the field-based tracking techniques. For the IR-10.8-µm it does not represent the convective growth phase well. However, for the HRV channel the representation of the convective growth is better and it agrees with the median growth phase of the manual tracking.

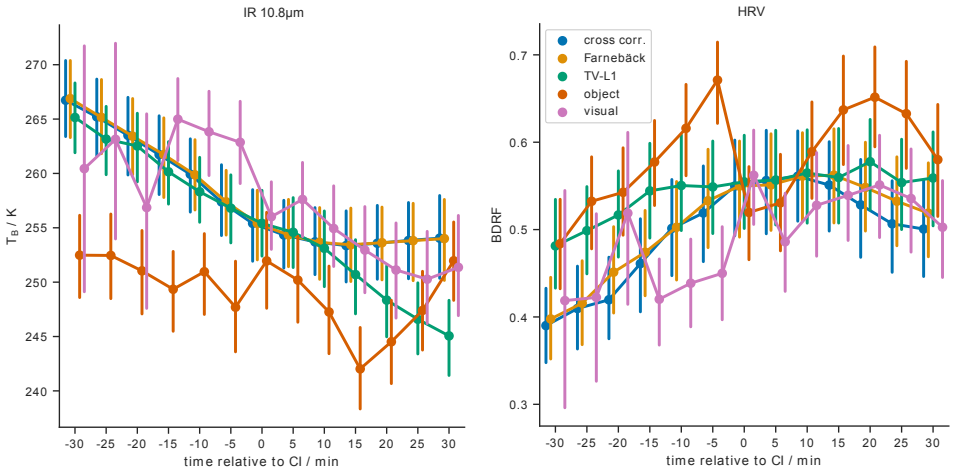

Figure 5: **Median growth phase representation (dot) and inter quantile range (error bar) of the database case for the different tracking techniques. The life cycle for the IR-10.8-µm channel is given as a brightness temperature and for the HRV channel as the bidirectional reflectivity factor (BDRF). The curves have been shifted on the time axis for the different techniques to enhance the visibility but belong to the same time steps.**

Applicability for CI detection

The rather reasonable representation of the convective life cycle growth phase above, looks promising regarding the application of the examined tracking techniques whithin a CI detection algorithm. Nevertheless, looking at the cloud top cooling rate (as a primary indicator for the cloud vertical growth), it turns out that the rather small deviations between the tracking techniques lead to large differences in the cloud top cooling rate. Taking the 5-min cloud top cooling rate derived from the IR-10.8-µm channel, a possible indication time step given by the different tracking techniques varies by 25 min (Fig. 6). Most of the techniques show a minimum in the cloud top temperature cooling rate of -3 K / 5 min to -4 K / 5 min which could be used as an indicator. But for the most techniques this minimum is quite broad. This hold true for the manual tracking and Farnebäck optical flow. For the cross correlation tracking the overall variation is quite large. There is a local minimum in cloud top cooling rate 10 min before the radar defined CI time step, which could mean an indication. There is a second minimum 15 min after the radar defined CI time step. So, the indication is not quite clear and the uncertainty is quite large. The median cloud top cooling rate derived using the Farnebäck optical flow has no clear minimum at all, but shows a very broad valley. So at this stage, none of the tracking approaches result in a clear indication for the cloud top cooling rate.

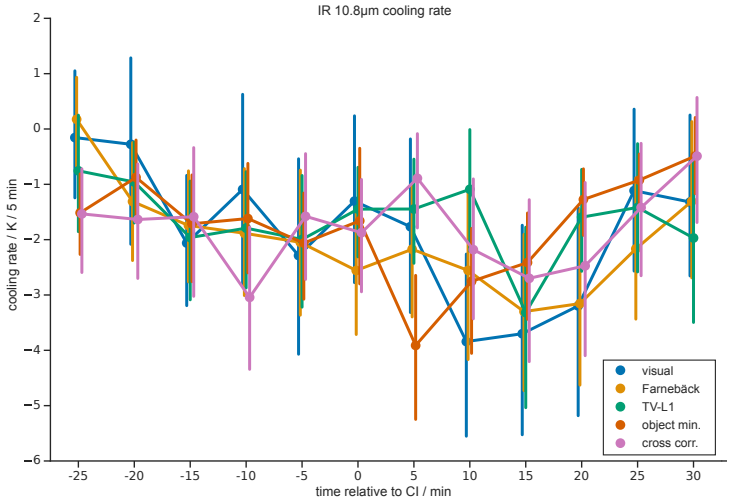

Figure 6: **Median 5 min IR 10.8 µm cooling rate of the database cases (dot) with inter quantile range (error bar) for the different tracking techniques. The curves have been shifted on the time axis for the different techniques to enhance the visibility but belong to the same time steps.**

CONCLUSION AND OUTLOOK

This study presents a preliminary analysis of the sensitivity of Lagrangian time trends on the detection of convective initiation (CI) used within a satellite based nowcasting algorithm. Using a manually created case database of tracks as a reference, and a radar based CI definition as starting point, four automatic tracking techniques have been analysed in terms of the tracking accuracy, the representation of the convective life cycle and their applicability for CI detection. The results show that the tracking errors of all field-based techniques are rather small and quite comparable in terms of tracking accuracy and the representation of the convective growth phase.

However, the case data base used in this study is quite small and needs to be extended to give statistical results. Also only one interest field was considered. The analysis of more interest fields will allow a clearer answer to the question how the tracking techniques affect the CI detection capability.

Another challenge is the definition of objects and their robust identification. The object definition used, is mainly targeted at the growth phase and the mature stage of the convective clouds. It works if the cloud field structure is not too complex, but fails in the case of complex cloud morphology. Especially in the early phase of the convective life cycle the cloud structure can be complex and thus the current approach does not cover this

stage well. To improve the object definition, a cloud type based approach seems promising. The approach to link the objects of subsequent time steps into one object track also needs improvement. The introduction of an advection correction is expected to improve this part of the object tracking substantially. Another promising idea seems to be the development of a combined strategy making use of field-based tracking during the early life cycle, and switching to object-based tracking once objects can be reliably detected.

References

Arnaud, Y., Desbois, M. & Maizi, J. (1992) Automatic tracking and characterization of African convective systems on Meteosat pictures. Journal of Applied Meteorology, **31**, pp. 443–453.

Autonès, F. & Moisselin, J.-M. (2016) Algorithm Theoretical Basis Document for Convection Products. Tech. rep., Météo France, NWC SAF, EUMETSAT.

Bedka, K. M. & Mecikalski, J. R. (2005) Application of Satellite-Derived Atmospheric Motion Vectors for Estimating Mesoscale Flows. Journal of Applied Meteorology, **44**, pp. 1761–1772.

Butler, D. J., Wulff, J., Stanley, G. B. & Black, M. J. (2012) A naturalistic open source movie for optical flow evaluation. In A. Fitzgibbon et al. (ed.), European Conf. on Computer Vision (ECCV), Part IV, LNCS 7577. Springer-Verlag, pp. 611–625.

Farnebäck, G. (2003) Two-frame motion estimation based on polynomial expansion. In Bigun, J. & Gustavsson, T. (eds.), Proceedings of the 13th Scandinavian conference on Image analysis (SCIA'03),. Springer-Verlag, Berlin, Heidelberg, pp. 363–370.

Fujita, T. T., Watanabe, K. & Izawa, T. (1969) Formation and structure of equatorial anticyclones caused by large-scale cross-equatorial flows determined by ATS-I photographs. Journal of Applied Meteorology, **8**, pp. 649–667.

Guizar-Sicairos, M., Thurman, S. T. & Fienup, J. R. (2008) Efficient subpixel image registration algorithms. Optics letters, **33**, pp. 156–158.

Haberlie, A. M., Ashley, W. S. & Pingel, T. J. (2015) The effect of urbanisation on the climatology of thunderstorm initiation. Quarterly Journal of the Royal Meteorological Society, **141**, pp. 663–675. doi:10.1002/qj.2499.

Janku, P., Koplik, K., Dulik, T. & Szabo, I. (2016) Comparison of tracking algorithms implemented in OpenCV. In MATEC Web of Conferences, vol. 76. EDP Sciences, p. 04031.

Machado, L., Rossow, W., Guedes, R. & Walker, A. (1998) Life cycle variations of mesoscale convective systems over the Americas. Monthly Weather Review, **126**, pp. 1630–1654.

Mathon, V. & Laurent, H. (2001) Life cycle of Sahelian mesoscale convective cloud systems. Quarterly Journal of the Royal Meteorological Society, **127**, pp. 377–406.

Mecikalski, J. R. & Bedka, K. M. (2006) Forecasting Convective Initiation by Monitoring the Evolution of Moving Cumulus in Daytime GOES Imagery. Mon. Wea. Rev., **134**, pp. 49–78. doi:10.1175/mwr3062.1.

Patou, M., Vidot, J., Riédie, J., Penide, G. & Garret, T. J. (2018) Prediction of the Onset of Heavy Rain Using SEVIRI Cloud Observations. Journal of Applied Meteorology and Climatology, **57**, pp. 2343–2361.

Pereda, J. G. & Calbet, X. (2016) Algorithm Theoretical Basis Document for the Wind product processors of the NWC/GEO. Tech. rep., AEMet, NWC SAF.

Roberts, R. D. & Rutledge, S. (2003) Nowcasting Storm Initiation and Growth Using GOES-8 and WSR-88D Data. Weather and Forecasting, **18**, pp. 562–584. doi:10.1175/1520-0434(2003)018<0562:nsiagu>2.0.co;2.

Senf, F. & Denke, H. (2017) Satellite-Based Characterization of Convective Growth and Glaciation and Its Relationship to Precipitation Formation over Central Europe. Journal of Applied Meteorology and Climatology, **56**, pp. 1827–1845.

Siewert, C. W., Koenig, M. & Mecikalski, J. R. (2010) Application of Meteosat second generation data towards improving the nowcasting of convective initiation. Meteorological Applications, pp. 422–451. doi:10.1002/met.176.

Urbich, I., Bendix, J. & Müller, R. (2018) A Novel Approach for the Short-Term Forecast of the Effective Cloud Albedo. Remote Sensing, **10**, pp. 1–16.

Van der Walt, S., Schönberger, J. L., Nunez-Iglesias, J., Boulogne, F., Warner, J. D., Yager, N., Gouillart, E. & Yu, T. (2014) scikit-image: image processing in Python. PeerJ, **2**, p. e453.

Walker, J. R., MacKenzie, W. M., Mecikalski, J. R. & Jewett, C. P. (2012) An Enhanced Geostationary Satellite–Based Convective Initiation Algorithm for 0–2-h Nowcasting with Object Tracking. J. Appl. Meteor. Climatol., **51**, pp. 1931–1949. doi:10.1175/jamc-d-11-0246.1.

Wu, Q., Wang, H.-Q., Lin, Y.-J., Zhuang, Y.-Z. & Zhang, Y. (2016) Deriving AMVs from Geostationary Satellite Images Using Optical Flow Algorithm Based on Polynomial Expansion. Journal of Atmospheric and Oceanic Technology, **33**, pp. 1727–1747.

Yen, J.-C., Chang, F.-J. & Chang, S. (1995) A new criterion for automatic multilevel thresholding. IEEE Transactions on Image Processing, **4**, pp. 370–378.

Zach, C., Pock, T. & Bischof, H. (2007) A Duality Based Approach for Realtime TV-L Optical Flow. In Hamprecht, F. A., Schnörr, C. & Jähne, B. (eds.), Pattern Recognition: 29th DAGM Symposium, Heidelberg, Germany, September 12-14, 2007, Proceedings, vol. 29. p. 560.
